International Journal of Disaster Risk Reduction 135 (2026) 106030

Contents lists available at ScienceDirect

International Journal of Disaster Risk Reduction

journal homepage: www.elsevier.com/locate/ijdrr

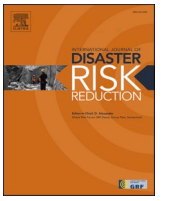

Complex network-based detection and forecasting of high-intensity tropical cyclones

Ziyu Jiang [a,c,d,1], Kaiwen Li [b,d,1], Ming Wang [a,f,*], Kai Liu [a,f], Shraddha Gupta [d,e], Jürgen Kurths [d,g]

[a] School of National Safety and Emergency Management, Beijing Normal University, 100875, Beijing, China
[b] School of National Security (School of Politics, Law and Public Administration), Shaanxi Normal University, 710119, Xi'an, China
[c] Faculty of Geographical Science, Beijing Normal University, 100875, Beijing, China
[d] Department of Complexity Science, Potsdam Institute for Climate Impact Research (PIK), 14473, Potsdam, Germany
[e] Department of Geography, Ludwig-Maximilians-Universität München, 80333, Munich, Germany
[f] Joint International Research Laboratory of Catastrophe Simulation and Systemic Risk Governance, Beijing Normal University at Zhuhai, 519087, Zhuhai, China
[g] Department of Physics, Humboldt-Universität zu Berlin, 10099, Berlin, Germany

A B S T R A C T

Accurate detection and forecasting of tropical cyclone tracks using limited climate variables and data is challenging. Here, we propose an innovative time-evolving complex network approach for detecting and forecasting high-intensity tropical cyclones (HITCs) based on mean sea level pressure and relative vorticity at 850 hPa. This approach enables us to successfully reproduce the tracks of HITCs of the Western North Pacific, achieving a mean detection rate exceeding 0.8 and a track error below 120 km in most cases. When applied to forecast 2023 HITC tracks using medium-range weather forecast data, we achieve a detection rate above 0.65 and a track error of less than 260 km for forecasts within 5 days. Our results highlight the strong potential of network-based approaches as data-integrative, physically interpretable statistical tools for HITCs detection and short-term forecasting, leveraging complex climate connectivity to enhance predictive skill.

1. Introduction

Tropical cyclones (TCs), especially those with high intensity, could cause a serious threat to the vulnerable dense coastal population of surrounding countries and island regions, leading to a substantial economic loss every year [1]. This is because TCs are usually accompanied by strong wind [2] and extreme rainfall [3,4], further triggering a series of secondary disasters such as floods [5] and landslides [6]. Among all ocean basins, the highest TC formation frequency is observed over the Western North Pacific (WNP), with a seasonal peak in frequency from May to November [7]. In such an active basin, multiple cyclone systems may form simultaneously. There has been an increase in the occurrence of severe cyclones in recent years due to global warming [8]. This has also increased the probability of occurrence of such multiple cyclone events. Therefore, TC tracking algorithms are essential for understanding, predicting, and mitigating the impacts of TCs. This can provide risk assessment and operational guidance for maritime and offshore activities.

Over the past few decades, previous studies have reached a consensus on the key ocean-atmospheric variables affecting the formation and development of TCs [9], including thermodynamic [10–12] and dynamic [13,14] variables. This has made TCs forecasting

* Corresponding author. School of National Safety and Emergency Management, Beijing Normal University, Beijing, China
E-mail address: wangming@bnu.edu.cn (M. Wang).
[1] Ziyu Jiang and Kaiwen Li are co-first authors, contributed equally to this work.

https://doi.org/10.1016/j.ijdrr.2026.106030
Received 15 August 2025; Received in revised form 19 January 2026; Accepted 25 January 2026
Available online 29 January 2026

more accurate and reliable through improved tracking algorithms, which integrate data from satellites and real-time observation systems with physical atmospheric models [15], advanced statistical techniques, and deep learning approaches [16,17]. Existing machine learning models typically rely on large-scale datasets and extensive training processes. However, forecasting remains highly challenging due to the complex dynamics governing TC tracks, which are influenced by multiple atmospheric and oceanic factors [18,19]. Given that TC tracks are part of a complex coupled system, there is a strong motivation to develop a data-driven tracking algorithm that leverages a small-sample-driven framework and effectively integrates spatiotemporal interactions influencing TC movement and intensity while maintaining reliability and accuracy.

Complex climate networks, based on graph theory [20,21], have proven to be powerful tools for characterizing the spatiotemporal organization pattern of climate variability [22]. They are constructed by assessing statistical relationships among the subcomponents (e.g., represented by geographical grids) in the climate system. Due to its inherent nonlinear and data-integrative nature, the method has been very successful in providing novel and efficient ways to improve predictive skill in El Niño Southern Oscillation (ENSO) [23], Indian Ocean Dipole (IOD) [24], droughts [25], or extreme precipitation [26,27] through detecting the spatial propagation pattern of droughts and extreme precipitation events and time-dependent relationship between ENSO or IOD and network metric. They have been used to capture the TC signatures, even in challenging scenarios such as the Fujiwhara interaction, where two cyclones in close proximity can influence each other's paths, complicating forecasts [28,29]. In this study, we utilize the potential of complex networks to develop a robust TC tracking and prediction scheme.

Here, we develop a time-evolving directed network framework to simulate the tracks of 369 high-intensity tropical cyclones (HITCs) during the TC season (from May to November) from 1979 to 2022. We evaluate our framework using detection rates and track error, comparing the simulated and observed tracks. Furthermore, we apply this method to forecast HITCs in 2023 using the ECMWF medium-range forecast system. Our findings demonstrate the potential of network-based approaches to provide novel insights into TC predictability, offering a promising tool for early warning and disaster preparedness through the lens of complexity science.

2. Data and Methods

2.1. Tropical cyclones and ocean-atmospheric variables

The TC best track dataset is obtained from China Meteorological Administration (CMA) [30,31]. The dataset records TCs over the WNP since 1949, including name, latitude, longitude, center minimum pressure, wind speed, and intensity at 6-h interval. All TCs can be classified into 6 levels based on their maximum wind speed during their lifetime. Here, only 369 HITCs are selected at TC season on

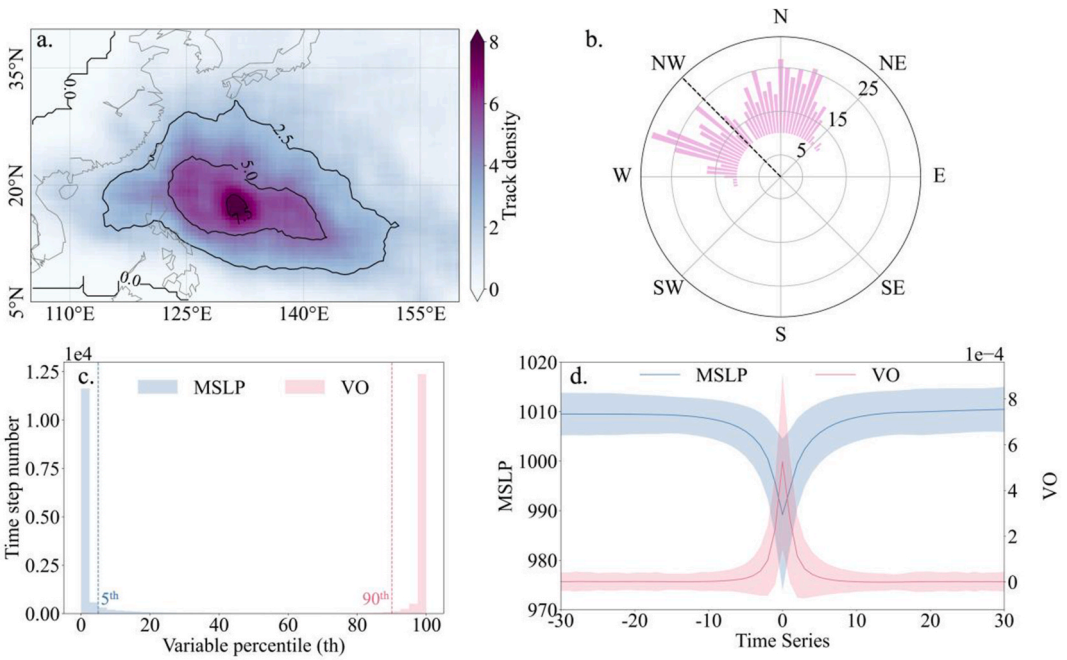

Fig. 1. Track density and movement direction of HITCs from 1979 to 2022, and temporal evolution and spatial pattern of related variables. **a** Track density of HITCs in past 44 years after uniform filter, and the high value located in the east ocean of the Philippines. **b** Movement direction between formation location and terminal location, the black line represents the average direction. The directions of almost all HITCs are between western and northeastern. **c** For HITCs, spatial percentile in each time step of MSLP and VO, the MSLP is less than 5th and VO is over 90th at most time step. **d** Temporal evolution of MSLP and VO at HITCs points center time step and slide forward/backward 30 time steps (shadow means 1 standard deviation), the MSLP and VO are also low value and high value in time series.

WNP (from May to November) from 1979 to 2022, including Severe Typhoon (STY) and Super Typhoon (SuperTY) with wind speeds over 41.5 m/s and 51 m/s respectively. For obtaining more convincing results, HITCs are used after 1979, as satellites are used to help monitor TCs after that [32,33]. On the WNP, tracks of HITCs are denser in the eastern of the Philippines (Fig. 1 (a)). And the movement direction of HITCs generally starting in the southeast and then moving northwest (Fig. 1 (b)), causing damage to coastal countries such as China, Japan and Southeast Asia.

The development of TCs is influenced by many thermodynamic and dynamic ocean-atmospheric variables [9,13], such as SST, humidity and so on. Among all these variables, mean sea level pressure (MSLP) and relative vorticity at 850 hPa (VO) are two key variables reflecting the evolution of TCs [34,35]. Here, MSLP and VO are obtained from the European Centre for Medium-Range Weather Forecast (ECMWF), Reanalysis 5 (ERA5) dataset [36,37] with $0.25^\circ \times 0.25^\circ$ spatial resolution, and 6h interval, corresponding to TCs best track dataset, at 00, 06, 12, 18 UTC every day.

TCs in the Northern Hemisphere are typically associated with low-pressure system and counterclockwise wind fields. Spatially, over 95 % HITCs correspond to MSLP values less than the 5th percentile and VO higher than the 90th percentile of the overall region (Fig. 1 (c)), and similar phenomena also occur in temporal patterns (Fig. 1 (d)). By comparing the evolution in MSLP and VO over 30 time steps (6h for a time step) before and after the HITCs time, it is evident that MSLP and VO expressed as low values and high values, respectively. These two variables respond well to the occurrence of HITCs, being basic variables for establishing evolving climate network. Specifically, we introduce temporal and spatial thresholds for MSLP and VO to jointly define HITCs events. The former considers the 5th percentile for MSLP and 99.5th percentile for VO of their sequences as temporal thresholds, while the latter uses the 5th percentile for MSLP and 90th percentile for VO of these values within the study area as regional thresholds. An event is defined as an HITC event only when atmospheric conditions simultaneously meet these spatial and temporal thresholds. For consecutive events, the initial occurrence is considered the time of the event.

Additionally, the ECMWF provides high-resolution forecast data with a lead time of up to 15 days, and the spatial resolution is consistent with reanalysis data. The forecasted meteorological variables include MSLP and VO. This forecast data will be used to establish evolving climate networks and predict the tracks of HITCs in 2023.

2.2. Event synchronization

Event synchronization (ES) is used to measure the synchronization between discrete events [38]. For two grids i and j, e_i and e_j represent the event series of these two grids, containing m and n events respectively. For e_i, an event u occurs time is e_i^u and an event v occurs time is e_j^v for e_j, where $u \in [1, m], v \in [1, n]$. The time delay between two events u and v is $t_{i,j}^{u,v} = e_i^u - e_j^v$. To ensure unique assignment of events, a dynamic time delay $\tau_{i,j}^{u,v}$ has been introduced:

$$\tau_{i,j}^{u,v} = \frac{min\left\{t_{i,i}^{u,u-1}, t_{i,i}^{u+1,u}, t_{j,j}^{v,v-1}, t_{j,j}^{v+1,v}\right\}}{2}$$

Besides, a maximum time delay $\tau_{max} = 8$ days is used to limit the time difference between two events. $q(i|j)$ represents the number of times an event occurs at grid i after an event occurs at grid j, its definition is as follows:

$$q(i|j) = \sum_{u=1}^{m} \sum_{v=1}^{n} S_{ij}^{uv}$$

With

$$S_{ij}^{uv} = \begin{cases} 1, if\ 0 < e_i^u - e_j^v < \min\left(\tau_{i,j}^{u,v}, \tau_{max}\right) \\ \frac{1}{2}, if\ e_i^u = e_j^v \\ 0, else \end{cases}$$

and for $q(j|i)$, it is analogous. ES strength between grid i and j is noted as $Q_{i,j}$, and it can be expressed as:

$$Q_{i,j} = \frac{q(j|i) - q(i|j)}{\sqrt{m \times n}}$$

where the value of $Q_{i,j}$ is between -1 and 1. When $|Q_{i,j}| = 1$, events between grid i and j are fully synchronized. Simultaneously indicate events at grid i occur always precede (follow) grid j. By introducing $Q_{i,j}$, we can identify the spatial propagation characteristic of HITCs and their temporal evolution patterns.

2.3. Evolving directed climate network

For each TC season from 1979 to 2022 (May to November), considering the lifecycle of TCs in the WNP is near 10 days, we divided it into 10-day time windows, with each day comprising four time steps (00, 06, 12, 18 UTC). The time windows slide with a step length of one day. The first time window is from April 22 to May 1, and the last time window is from November 30 to December 9. So there are

223 time windows every year. But only time windows including HITCs are further extracted. For each time window, a directed climate network is designed using ES. And only ocean grids are considered, because the MSLP field from ERA5 is more precise over the ocean than landfall. This is of great importance to shipping and offshore operations.

Evolving directed climate networks consist of 9812 sub-networks. In a single network, the ocean grids are seen as nodes, the weight of edges is the ES strength between two nodes. Weighted in-degree d_{in}^{i} refers to the sum of the weights of all edges directed towards grid i. Weighted out-indegree d_{out}^{i} means the sum of the weights of all edges that grid i direct towards other grids. To determine the spatial propagation patterns of HITCs events, network divergence ΔS is introduced as follows:

$$\Delta S = d_{out}^{i} - d_{in}^{i}$$

Positive divergence means a grid prefers to be directed toward other grids, and can be considered as a source region while negative divergence is the converse, and is a sink region.

The source region is always located around the early stage of a HITC, while the sink region is around the later stage in an evolving network. The symmetric patterns between such source and sink regions may represent the mapping of HITCs' evolutionary processes in the climate network.

For the 2023 forecasts, we applied the same framework, replacing reanalysis MSLP and VO with ECMWF high-resolution forecasts for the corresponding forecast future days, thereby making the approach directly transferable to an operational forecast. As the time window slide with 1 day, the initial forecast time shifts accordingly.

2.4. Significance tests

The significance test is applied to remove some weak edges, preventing disruption to the overall networks. To estimate the significance of the edge with synchronization strength Q_{ij}, 1000 pairs of surrogate event series are generated and then a null-model distribution is obtained. The number of events in these event series is the same as the number of events at two grids i and j, that is m and n respectively. The distribution of these events is uniform and random. Thus, there are 1000 ES strength values are derived for each edge, and the 99.5th of these values are considered as significant thresholds. Only when the $|Q_{ij}|$ is over the 99.5th values of 1000 ES values, the edge can be saved.

2.5. Robust tests

The τ_{max} is a key parameter of ES and affects the network structure. Previous studies have shown that τ_{max} has minimal impact on the network structure [27,39]. However, since the directed networks of TCs is a less explored field, we have measured the changes in network structure under different τ_{max} setting. In this study, we found that higher τ_{max} means there are more edges with long geographical distance. Because for HITCs, a longer time corresponds to a longer distance moved. So τ_{max} = 8,10 days are compared, corresponding to 32 and 40 time steps with 6h interval per time step. Jaccard Similarity Coefficient [40] is used to compare the similarity and difference between networks by calculating the ratio of the intersection of edges between two networks to the union of their edges. The higher the coefficient value, the greater the similarity between the samples. The result shows that the Jaccard Similarity Coefficient is 1 for most networks from 1979 to 2022, which means under different τ_{max}, the network is robust (Fig. 2).

2.6. Track simulation and result evaluation

Track simulation is based on the bank-like spatial pattern of network divergence because the divergence reflects the center region of the HITCs. The center line is skeletonized for each center region of HITCs, using a digital image process method (skeletonization). Finally, the center line is considered as the simulated tracks of HITC.

To evaluate the similarity of simulated tracks and observed tracks, two metrics are proposed, they are detection rate and track

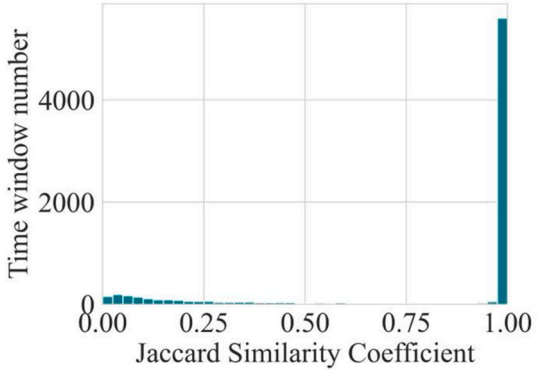

Fig. 2. Jaccard Similarity Coefficient of τ_{max} = 8,10 days. For different τ_{max}, networks are similar.

error. The detection rate means the proportion of HITCs points contained within the network divergence area relative to the total number of HITCs points. A higher value of this metric indicates that the evolving directed climate network is better at capturing the tracks of HITCs.

Geographical distance error between simulated tracks and observed tracks is evaluated using a pointwise distance-based track match approach, which is commonly adopted in operational numerical model forecast. In this study, the observed HITCs are treated as the reference, consisting of a sequence of discrete positions at regular temporal intervals. The simulated track derived from the proposed method is represented by a continuous centerline extracted from the identified HITCs region through skeletonization, typically composed of densely distributed spatial points. For each observed track point, the nearest point along the simulated centerline is identified based on the minimum geographical distance. The position error at that time step is then calculated as the haversine distance between two points. This procedure is repeated for all available observed track points. The track error is computed as the mean of these pointwise geographical distances.

3. Results

3.1. Evolving climate network for revealing the evolution of high-intensity tropical cyclones

In WNP (5°N-40°N, 105°E−160°E), 369 HITCs occurred in each TCs peak season from 1979 to 2022. HITCs consist of Severe Typhoon (STY) and Super Typhoon (SuperTY), with a maximum wind speed exceeding 41.5 m/s and 51 m/s respectively. The meteorological characteristics of all these HITCs are more pronounced compared to low-intensity TCs, featuring lower MSLP and higher VO. We define the intersection of a low MSLP and a high VO event in space and time as HITC events. Here, time-evolving climate networks are constructed using ES, which characterizes the temporal relationships between TC events at different locations (2. Data and Methods section '2.2. Event synchronization'). Nodes and edges in the network represent the geographical grids and synchronization strength between any two grids separately. Only significant edges are saved with $p < 0.005$ after analyzing 1000 surrogate random networks. (2. Data and Methods section '2.4. Significance tests'). We compute the spatial divergence for each network to identify the potential tracks of TCs. The spatial distribution of the network divergence ΔS is used to identify the center region and the evolution of HITCs, with positive (negative) ΔS values indicating the source (sink) region, and therefore, the propagation direction of these HITCs can be potentially identified.

In order to track the development of HITCs, ΔS of the corresponding time window is calculated for each HITC. Fig. 3 shows typical examples for three basic situations that may arise in the WNP basin during the lifetime of a HITC: 1) there is only 1 HITC in all related time windows during its lifetime, 2) more than 1 HITC occur around the same time period, but their tracks do not intersect, 3) more than 1 HITC occur, but their tracks intersect. These results show that ΔS derived from the directed climate network in each time

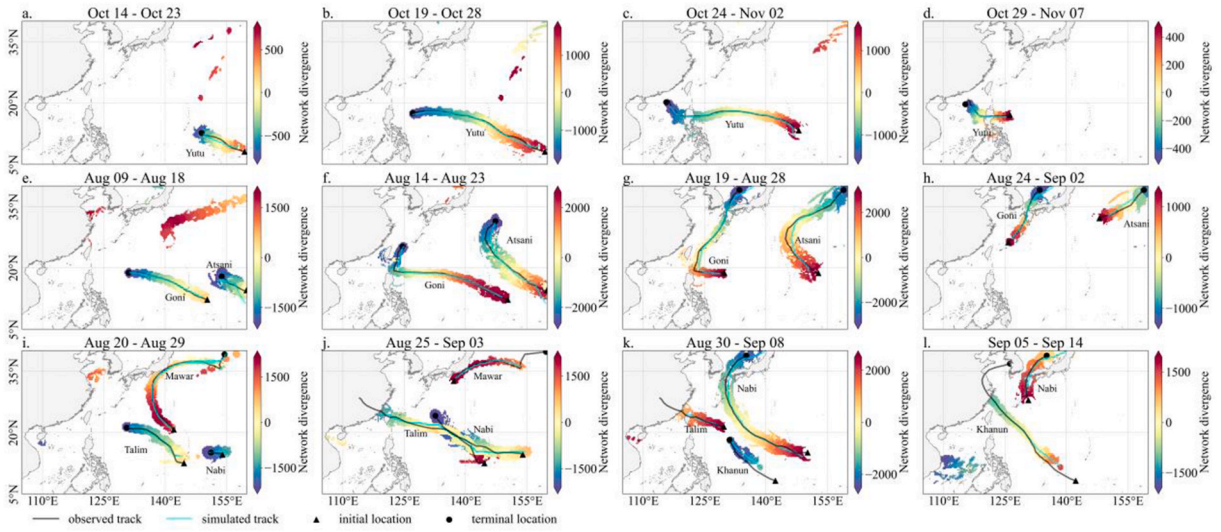

Fig. 3. Track detection of three typical situations of high-intensity TCs (HITCs) captured by network divergence. Relative high network divergence indicates earlier developmental stage of a HITC. Network divergence values transition towards relatively low values as the cyclone progresses to later stages. Black lines are observed tracks from China Meteorological Administrator (CMA) data, while cyan lines depict simulated tracks. **a-d** Only 1 HITC "Yutu" present in all time windows between October 14 to November 7, 2018. The network divergence indicates the core region of the HITC and the simulated tracks highly resemble with observations. **e-h** Two HITCs "Goni" and "Atsani" formed simultaneously from August 9 to September 2, 2015. These two HITCs are at sufficient distance from each other so as not to influence each other during their lifetime, and can be captured by spatial distribution of network divergence. **i-l** Network time windows from August 20 to September 14, 2005, shows development of four HITCs, "Mawar", "Nabi", "Talim" and "Khanun". Although "Nabi" and "Talim" influence each other in some stages, network divergence can effectively detect their tracks.

window reveals the evolution of HITCs and captures the center region around their tracks. For almost all HITCs, ΔS reflects their spatial pattern at different developmental stages even when TCs move closer to the coast. However, during the initial stage of HITCs, TC signatures are not easy to capture. This is because they are in their initial stages of development when their intensity is still relatively weak, and the changes in the magnitude of the MSLP and VO values are relatively small to be detected. Spatially, there is a gradual transition of ΔS around the tracks of HITCs from positive to negative as HITCs progress. This transition suggests that the directionality of the geographical grids comprising HITCs in the network from the early stages to the later stages of the development of the HITCs in a single time window is consistent with their propagation direction. The spatial pattern of network divergence also reflects the spatial and temporal evolution of underlying MSLP and VO. The low MSLP field and high VO field propagate coherently in space and time along the observed track, thereby leading to network divergence transition.

For a single HITC, ΔS around its track typically transitions from positive to negative as it progresses, for example in situations 1) and 2). This occurs because most of the connections are present at the grids neighboring the cyclone. However, there are also some exceptions. When two HITCs form during similar time periods and are in close proximity as in Fig. 3 (k), ΔS for one HITC may be almost totally positive (HITC "Talim") or totally negative (HITC "Khanun"), because connections may occur between these two HITCs. "Talim" occurred earlier than "Khanun", so ΔS is shown as from "Talim" to "Khanun". Although these two HITCs interact, the interactions vary at different stages of the HITCs, making ΔS transition from relatively high values to low values, which enables us to capture their tracks. Besides, when two HITCs intersect as in situation 3), the regions of the network divergence merge together making it hard to distinguish between the individual HITCs, e.g., "Talim" and "Nabi" in Fig. 3 (j). However, this intersection persists only until some developmental stages of the HITCs. From August 20 to September 14, 2005, there are four distant HITCs that develop in the basin during the same time period, then come in close proximity for some time, and finally separate again. We demonstrate that our evolving climate network-based approach can effectively deal with such complex scenarios and reliably detect HITCs tracks.

The larger deviations between the simulated tracks and the observed in some cases (Fig. 3) mainly occur during the early stages of HITCs development. During this phase, cyclones are typically weaker and less organized, with shallow pressure minima and less coherent vortex structures, which makes accurate center identification more challenging. It has been well documented that reanalysis products tend to underestimate TCs intensity and exhibit larger uncertainties in representing weak and developing systems, particularly in MSLP [41]. In Fig. 3 (a)–(c), some grid points distant from the HITCs, especially those in the northeast, are associated with significant network divergence. Although there are no HITCs in these grid points, they have low MSLP and high VO, leading to events similar to HITCs being falsely detected. Moreover, some areas near the sea-land boundary also experience some disturbances (Fig. 3 (e)), however since this study only considers ocean grid points, it reduces some of the potential connections between ocean and land grids. Additionally, we discovered that apart from the HITCs focused on in this study, some TCs of lower intensity, for example the track near Japan in Fig. 3 (e), can also be identified especially those slightly less intense than the HITCs.

3.2. Track simulation and evaluation

Network divergence of evolving climate networks can effectively capture the various developmental stages of HITCs. For a single HITC, the time duration of each climate network constructed is 10 days, and evolves with a shift in time step of 1 day. The choice of 10 days is sufficient to cover the average lifetime of a HITC in this basin. During the lifetime of a HITC, the network divergence transitions from relatively high to low values of ΔS making detection of HITC tracks possible. The simulated cyclone tracks are obtained by skeletonization of the corresponding network divergence field using digital image processing. To evaluate the difference between the simulated tracks and the observed tracks, the detection rate and track error are calculated. The results show that the simulated tracks are very close to observed tracks. The mean detection rate of all time windows is 0.82, and skewness and kurtosis show that most time windows are higher than 0.8 (Fig. 4 (a)). The track errors of all time windows are obtained by pointwise matching, and our results show that more than 75 % of time windows have track errors less than 120 km (Fig. 4 (b)). However, there are large deviations in some cases

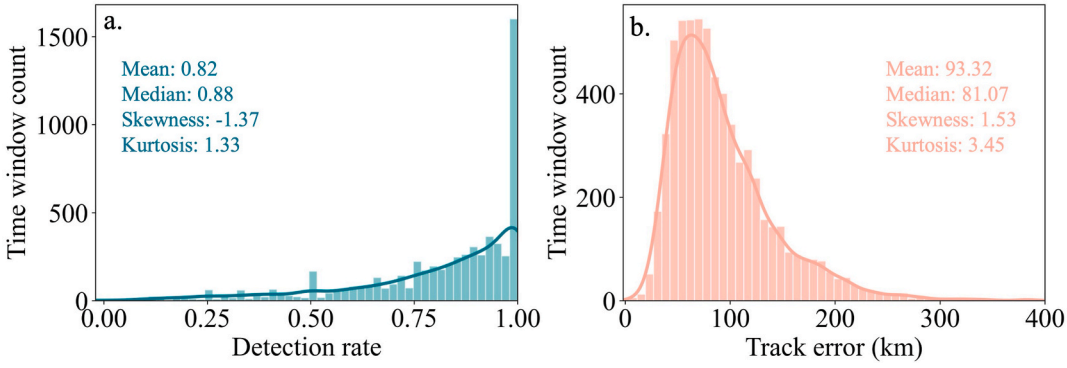

Fig. 4. Detection rate and track error of simulated tracks of time windows of HITCs from 1979 to 2022. **a** The result shows more than 80 % HITCs points can be captured by network divergence, with detection rate concentrated above 0.8 and small amount of values less than 0.5. This means the framework can capture the center region of HITCs efficiently. **b** The track error between simulated tracks and observed tracks of more than 75 % time windows are smaller than 120 km, which presents the simulated tracks are closely match with observed tracks.

(approx. 150 km) between the simulated and observed tracks when the HITCs abruptly change direction (Fig. 3 (g)). Moreover, when two HITCs come in close proximity (Fig. 3 (j)), the overlap of their divergence region results in a single simulated track and not two individual tracks as they should be. Although such uncertainty arising due to time-lagged overlap of tracks rarely occurs, and detection of single HITCs can usually be identified in later stages from subsequent networks. Overall, our results demonstrate that the directed climate networks employed in this study can effectively locate the core region of the HITCs using only MSLP and VO data. Therefore, our approach can be used to accurately simulate their propagation tracks.

3.3. High-intensity TCs forecast in 2023

In the past 44 years, 369 HITCs have been demonstrated to be effectively captured by time-evolving directed climate networks using only information from MSLP and VO data. In recent decades, numerical weather prediction models have achieved high resolution and great precision which have improved their forecasting skills, such the medium-range forecasts system data provided by ECWMF and along with neural network models like Pangu [42] and GraphCast [43]. In this part, using the directed evolving networks of 2023, we attempt to forecast HITC tracks 1–10 days ahead based on the forecast MSLP and VO data obtained from ECMWF. This enables us to validate the potential of our network-based framework to detect future HITCs in forecast data.

9 HITCs occurred in 2023, among which we first focus on simulating forecast tracks of Super Typhoon (SuperTY) “Doksuri” and “Khanun” (Fig. 5). SuperTY “Doksuri” caused severe damage to some countries around the Maritime continent and southeastern parts of China. “Doksuri” resulted in 2.95 million people affected and direct economic losses amounting to 1.94 billion euros [44]. The tracks of HITCs, such as “Khanun” abruptly changed directions due various environmental factors causing large uncertainties in track forecasts [45]. For exploring the effectiveness of our HITCs capture framework combing short-term high-resolution forecast data, we forecast the tracks of these two HITCs. The number of forecast days refers to the days of forecast data within a 10-day time window. As an example, for a forecast horizon of 1 day, the data for the first 9 days in the 10-day network time window is taken from ERA5, while the last day is from the ECMWF medium-range forecasting system high-resolution forecast data. When the number of forecast days in a window is small, the simulated and observed tracks almost highly resemble. As networks are constructed over longer forecast horizons, the track error of the simulated tracks gradually increases. However, for “Doksuri” and “Khanun”, the track detection performance of the 5-day forecasts is equivalent to that of 1-day forecast (Fig. 5 (e)). We also observe that the deviation between the simulated and observed tracks are around 200 km for networks representing longer forecast horizons which do not reply on reanalysis data (Fig. 5 (j)), which also suggests that the framework has strong potential applications for HITCs tracks forecasting and warning.

The detection rate and track error are also computed for time windows related to each HITC. Fig. 6 shows both metrics from forecast 1–10 days for each HITC in 2023. For 8 HITCs except “Doksuri”, as the time covered by the forecast data increases, the detection rate of HITCs points shows a gradually significant decrease down to 0.49 (“Koinu” HITC) when forecast days is 10. As mentioned above, “Doksuri” is a counter example indicating rare cases where detection of the cyclone using our network-based framework is effective even when relying solely on forecast data (Fig. 5 (j)). This may be associated to the fact that the forecast data from global models such as the ECMWF-IFS system perform better for longer-term forecasts [46]. As in most forecasting systems, the difference between the simulated and observed tracks gradually increases as the number of forecast days increases, which is also related to the fact that the forecast accuracy of the underlying variables decreases as lead time increases. However, the track error is a maximum of 260 km (“Haikui” HITC) at forecast 10 days. In addition, we also find a non-significant increase in the track error of

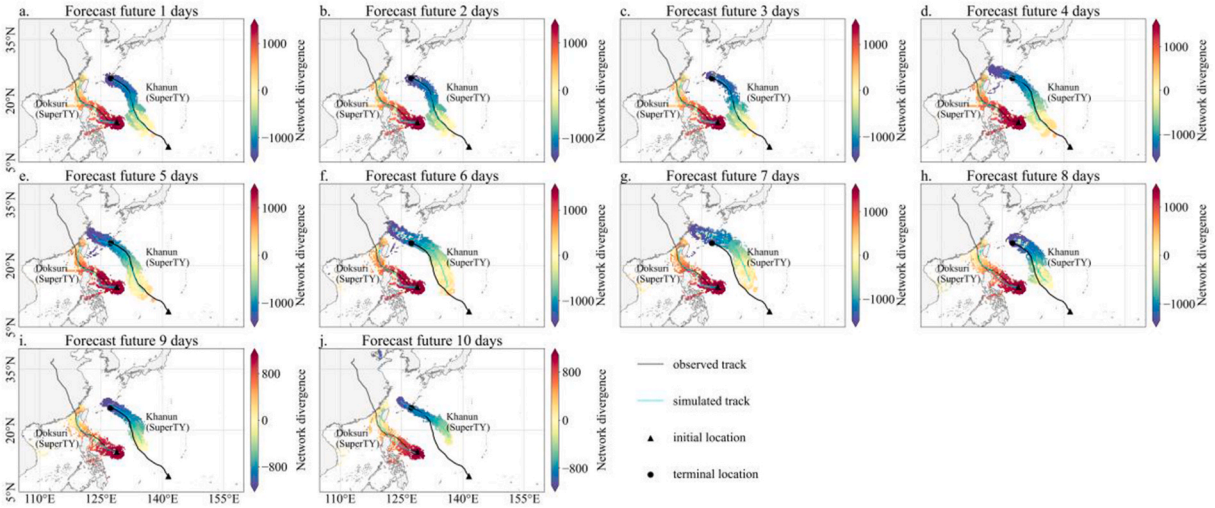

Fig. 5. An example of forecast time window of July 23 to August 1, 2023, and the forecast future days are from 1 day to 10 days. The black/cyan lines are observed/simulated tracks correspondingly. There are two HITCs in this time window, they are “Doksuri” and “Khanun”, and the formation time of “Doksuri” is earlier than “Khanun”. With the number of forecast days increase, the deviation between observed tracks and simulated tracks gradually increases, especially for the SuperTY “Khanun”.

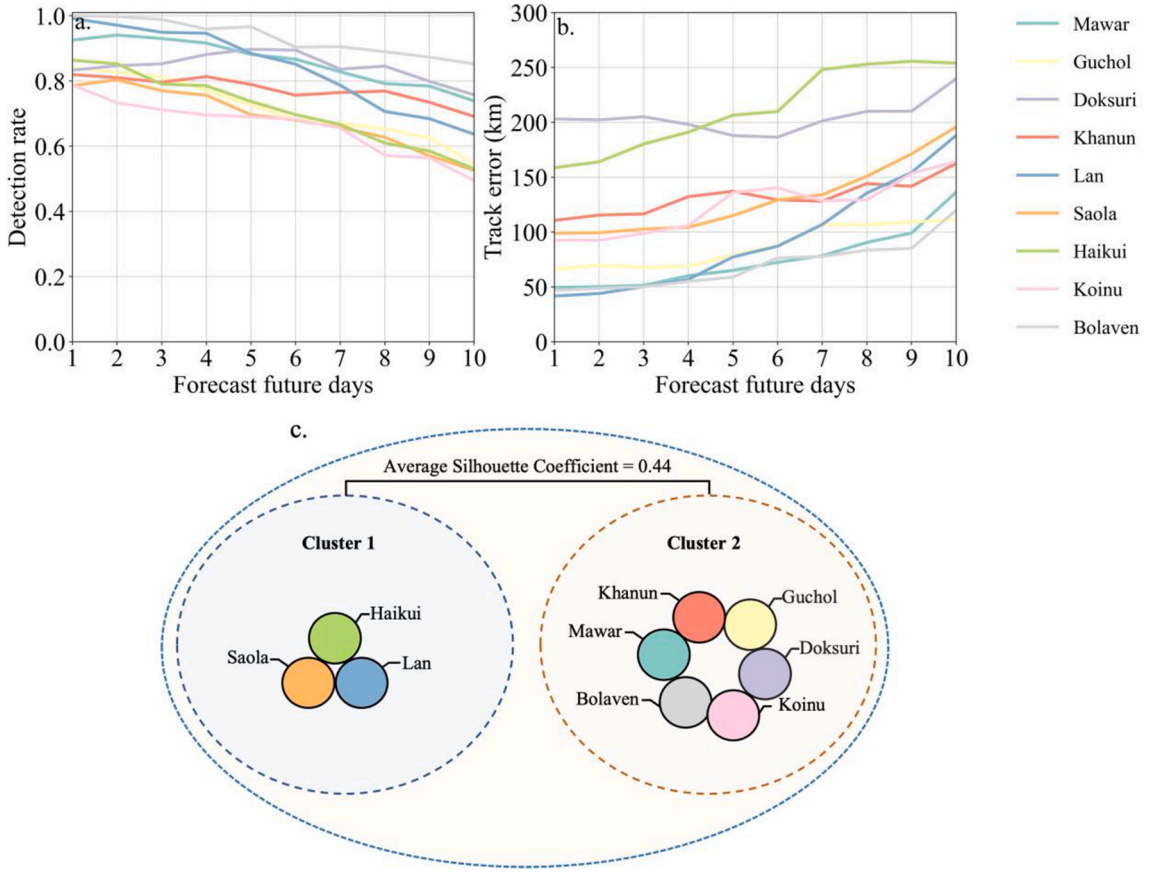

Fig. 6. Detection rate and track of 9 forecast HITCs for forecast days from 1 to 10 days and cluster of these HITCs. **a** Detection rate of 9 HITCs as forecast days increase. The detection rate gradually decreases as additional forecast data is incorporated, and the smallest detection rate is around 0.5 of "Koinu" when all data in this time window is forecast data. **b** The evolution of track error with different forecast days. As the number of forecast days increase, the track error gradually increases and up to around 260 km for "Haikui" at forecast 10 days. **c** K-means clustering results of 9 HITCs based on detection rate and track error with the Average Silhouette Coefficient of 0.44. "Saola", "Lan" and "Haikui" are divided as cluster 1, and others are cluster 2.

"Doksuri" (Supplementary Material Table 1). For the forecast cases shown in Fig. 5, the increasing track deviations with forecast days are closely associated with the growing errors in the forecast MSLP and VO field evaluated by the Bias, Root Mean Square Error (RMSE) and Anomaly Correlation Coefficient (ACC) (Fig. 7). Considering detection rate and track error, all these HITCs are clustered to 2 classes, with the Average Silhouette Coefficient of 0.44. The first cluster includes HITCs "Saola", "Lan" and "Haikui", which exhibit a more pronounced increase in track error and decrease in detection rate as the forecast period increases. The track error trend of these three HITCs are more than 10 km/day. The remaining HITCs from 2023, which display a more linear trend in track error relative to the number of forecast days, are grouped into the second cluster.

Although representative results for 2023 are shown here, the evaluation is also conducted for HITCs during 2022–2024, with detailed results provided in the Supplementary Material Figs. 1–4, and they are similar with the results of 2023. Besides, a benchmark comparison with ECMWF and NCEP using the track error is conducted (see Supplementary Material Table 2). The ECMWF and NCEP generally achieve smaller track errors at shorter forecast days. But with the forecast days increases, the track error calculated between simulated tracks proposed in this study and observed exhibits a more stable error growth.

4. Discussion and conclusion

A time evolving directed climate networks approach based on pressure and vorticity data is developed to reveal the evolution of HITCs from 1979 to 2022 during the TCs season in WNP. The network divergence ΔS shifts from positive to negative around the HITCs tracks, aiding their effective track capture. The simulated HITCs tracks are extracted through skeletonization based on the center region depicted by ΔS. The results show that the framework achieves a mean detection rate of 0.82, and the track error of more than 75 % of time windows is less than 120 km. Furthermore, the method is used to forecast HITCs tracks in future 1–10 days for the 2023 events based on the high-resolution forecast data. The framework reached here a detection rate up to 0.85 and track error less than 260 km when using forecast data of 10 days all HITCs in 2023. The detection rate decreases with increasing forecast days and the track

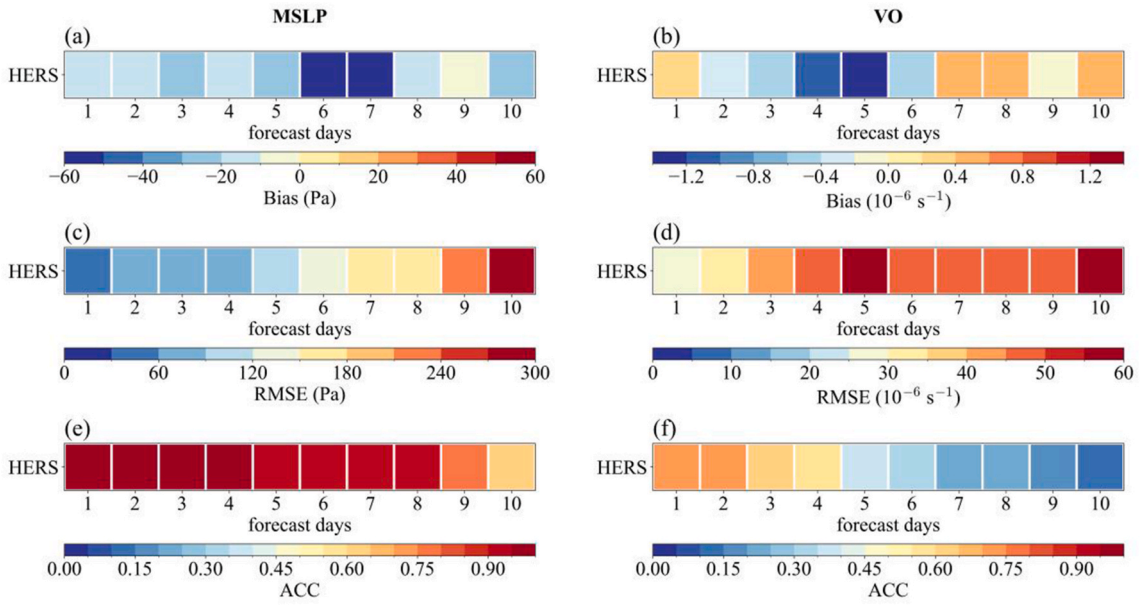

Fig. 7. Forecast errors of mean sea level pressure (MSLP) and relative vorticity at 850 hPa (VO) from forecast 1–10 days, evaluated by comparing ECMWF HERS with ERA5. **a-b** the mean Bias of MSLP and VO. **c-d** Root Mean Square Error (RMSE) of MSLP and VO. **e-f** Anomaly Correlation Coefficient (ACC) of MSLP and VO.

error shows the opposite result, introducing crucial insight for HITCs forecast. A benchmark comparison with operational numerical models indicates that ECMWF and NCEP generally achieve smaller track errors at short forecast lead times (approximately 6 days), benefiting from high-resolution dynamical frameworks and data assimilation systems. As forecast lead time increases, the proposed evolving directed climate network approach exhibits a more gradual and stable error growth, reflecting its capability to capture the large-scale structural evolution of HITCs tracks from a network topology perspective.

Although the algorithm has its limitations for it struggles to capture HITC tracks in cases when they are in their early stages of formation and relatively weak intensity or when multiple HITCs in close proximity interact with each other. In spite of these challenges, which are faced by majority of the existing tracking algorithms, our evolving directed climate network approach was able to efficiently capture the HITC tracks from 1979 to 2022, and forecast tracks in 2023.

Here, we focus on a short and medium-range forecast based on the framework which incorporates data and the assessment of statistical interactions between geographical grids arising from shared underlying physical processes. The method achieves an accurate estimation and detection of HITCs without the need for a large number of training samples like machine learning approaches. With the accelerating growth of meteorological AI big models, our framework can provide physical constraints to deep learning methods, enhancing interpretability. We have conducted experiments using AI big models, including Pangu and FuXi, and the results demonstrate that the proposed network-based framework can be naturally integrated with large-scale DL models to provide forecast tracks and capture HITCs central region (see Supplementary Material). Several key directions can extend the ability of this approach. A promising application of this algorithm is that it can be applied to get robust projections of TC tracks in different ocean basins under future warming scenarios, enhancing long-term climate risk assessment and policy formulation. Moreover, incorporating large-scale climate patterns, such as ENSO [47,48], could improve the multi-scale predictability of HITCs. In future work, we will further refine this method to enable accurate detection and forecast across different TCs intensity and of their intensities. By utilizing the spatio-temporal connectivity of the climate system, this method provides a novel perspective on detection of propagation patterns of extreme events like cyclones, with implications for early warning systems, disaster preparedness, and climate adaptation strategies.

CRediT authorship contribution statement

Ziyu Jiang: Writing – review & editing, Writing – original draft, Visualization, Software, Methodology, Conceptualization. **Kaiwen Li:** Writing – review & editing, Writing – original draft, Visualization, Software, Methodology, Conceptualization. **Ming Wang:** Writing – review & editing, Supervision, Methodology, Funding acquisition, Conceptualization. **Kai Liu:** Writing – review & editing, Methodology. **Shraddha Gupta:** Writing – review & editing, Methodology. **Jürgen Kurths:** Writing – review & editing, Methodology, Conceptualization.

Code availability

Python is used for coding and drawing plots. The code used in this study is available from the corresponding author or reasonable

request.

Declaration of competing interest

The authors declare that they have no known competing financial interests or personal relationships that could have appeared to influence the work reported in this paper.

Acknowledgments

The authors are grateful to Prof. Niklas Boers, Dr. Yu Huang, Dr. Fenying Cai, Dr. Jianxin Zhang for their helpful suggestions. The authors are grateful to ECMWF for providing the forecast data. The research for this article is supported by the National Natural Science Foundation of China (No. 52394232), National Key R&D Program of China (No. 2024YFC3014100), and Fundamental Research Funds for the Central Universities (No. 2243300007). Furthermore, the authors gratefully acknowledge the Ministry of Research, Science and Culture (MWFK) of Land Brandenburg for supporting this project by providing resources on the high-performance computer system at the Potsdam Institute for Climate Impact Research.

Appendix A. Supplementary data

Supplementary data to this article can be found online at https://doi.org/10.1016/j.ijdrr.2026.106030.

Data availability

TC best track data is available from the CMA at https://tcdata.typhoon.org.cn/zjljsjj.html. MSLP and VO reanalysis data are derived from ERA5 at Catalogue — Climate Data Store (copernicus.eu) (https://cds.climate.copernicus.eu/datasets). MSLP and VO forecast data need to be requested from ECMWF at ECMWF | MARS Catalogue (https://apps.ecmwf.int/mars-catalogue).

References

[1] L. Qin, L. Zhu, X. Liao, C. Meng, Q. Han, Z. Li, S. Shen, W. Xu, J. Chen, Recent northward shift of tropical cyclone economic risk in China, Npj Nat. Hazards 1 (2024) 8, https://doi.org/10.1038/s44304-024-00008-9.
[2] P.R. Sparks, Wind speeds in tropical cyclones and associated insurance losses, J. Wind Eng. Ind. Aerod. 91 (2003) 1731–1751, https://doi.org/10.1016/j.jweia.2003.09.018.
[3] A. Miniussi, G. Villarini, M. Marani, Analyses through the metastatistical extreme value distribution identify contributions of tropical cyclones to rainfall extremes in the Eastern United States, Geophys. Res. Lett. 47 (2020), https://doi.org/10.1029/2020GL087238.
[4] F. Cai, S. Yang, Z. Wang, J. Chen, J. Wang, W. Chen, Triggering effect of an unusual northwestward-moving tropical cyclone over the Bay of Bengal on the extremely early Indian summer monsoon onset, Clim. Dyn. 61 (2023) 621–631, https://doi.org/10.1007/s00382-022-06603-8.
[5] A. Rajeev, V. Mishra, On the causes of tropical cyclone driven floods in India, Weather Clim. Extrem. 36 (2022) 100432, https://doi.org/10.1016/j.wace.2022.100432.
[6] J. Cogan, I. Gratchev, G. Wang, Rainfall-induced shallow landslides caused by ex-Tropical Cyclone Debbie, 31st March 2017, Landslides 15 (2018) 1215–1221, https://doi.org/10.1007/s10346-018-0982-4.
[7] A.H. Sobel, A.A. Wing, S.J. Camargo, C.M. Patricola, G.A. Vecchi, C. Lee, M.K. Tippett, Tropical cyclone frequency, Earths Future 9 (2021), https://doi.org/10.1029/2021EF002275.
[8] M. Stowasser, Y. Wang, K. Hamilton, Tropical cyclone changes in the Western north Pacific in a global warming scenario, J. Clim. 20 (2007) 2378–2396, https://doi.org/10.1175/JCLI4126.1.
[9] W.M. Gray, The formation of tropical cyclones, Meteorl. Atmos. Phys. 67 (1998) 37–69, https://doi.org/10.1007/BF01277501.
[10] J.L. Evans, Sensitivity of tropical cyclone intensity to Sea surface temperature, J. Climate 6 (1993) 1133–1140, https://doi.org/10.1175/1520-0442(1993)006%253C1133:SOTCIT%253E2.0.CO;2.
[11] K.J. Tory, R.A. Dare, Sea surface temperature thresholds for tropical cyclone Formation, J. Clim. 28 (2015) 8171–8183, https://doi.org/10.1175/JCLI-D-14-00637.1.
[12] L. Wu, H. Su, R.G. Fovell, B. Wang, J.T. Shen, B.H. Kahn, S.M. Hristova-Veleva, B.H. Lambrigtsen, E.J. Fetzer, J.H. Jiang, Relationship of environmental relative humidity with North Atlantic tropical cyclone intensity and intensification rate, Geophys. Res. Lett. 39 (2012), https://doi.org/10.1029/2012GL053546.
[13] K.J. Tory, R.A. Dare, N.E. Davidson, J.L. McBride, S.S. Chand, The importance of low-deformation vorticity in tropical cyclone formation, Atmos. Chem. Phys. 13 (2013) 2115–2132, https://doi.org/10.5194/acp-13-2115-2013.
[14] W. Na, Z. Xinghai, C. Lianshou, H. Hao, Comparison of the effect of easterly and westerly vertical wind shear on tropical cyclone intensity change over the western North Pacific, Environ. Res. Lett. 13 (2018) 034020, https://doi.org/10.1088/1748-9326/aaa496.
[15] T. Islam, P.K. Srivastava, M.A. Rico-Ramirez, Q. Dai, M. Gupta, S.K. Singh, Tracking a tropical cyclone through WRF–ARW simulation and sensitivity of model physics, Nat. Hazards 76 (2015) 1473–1495, https://doi.org/10.1007/s11069-014-1494-8.
[16] L. Wang, B. Wan, S. Zhou, H. Sun, Z. Gao, Forecasting tropical cyclone tracks in the northwestern Pacific based on a deep-learning model, Geosci. Model Dev. (GMD) 16 (2023) 2167–2179, https://doi.org/10.5194/gmd-16-2167-2023.
[17] Y. Wang, L. Han, Y.-J. Lin, Y. Shen, W. Zhang, A tropical cyclone similarity search algorithm based on deep learning method, Atmos. Res. 214 (2018) 386–398, https://doi.org/10.1016/j.atmosres.2018.08.018.
[18] E. Walker, D. Mitchell, W. Seviour, The numerous approaches to tracking extratropical cyclones and the challenges they present, Weather 75 (2020) 336–341, https://doi.org/10.1002/wea.3861.
[19] L. Magnusson, J.D. Doyle, W.A. Komaromi, R.D. Torn, C.K. Tang, JohnnyC.L. Chan, M. Yamaguchi, F. Zhang, Advances in understanding difficult cases of tropical cyclone track forecasts, Trop. Cycl. Res. Rev. 8 (2019) 109–122, https://doi.org/10.1016/j.tcrr.2019.10.001.
[20] D.B. West. Introduction to Graph Theory, Prentice Hall, Upper Saddle River, 2001.
[21] J. Fan, J. Meng, J. Ludescher, X. Chen, Y. Ashkenazy, J. Kurths, S. Havlin, H.J. Schellnhuber, Statistical physics approaches to the complex Earth system, Phys. Rep. 896 (2021) 1–84, https://doi.org/10.1016/j.physrep.2020.09.005.

[22] F. Cai, C. Liu, D. Gerten, S. Yang, T. Zhang, K. Li, J. Kurths, Sketching the spatial disparities in heatwave trends by changing atmospheric teleconnections in the Northern Hemisphere, Nat. Commun. 15 (2024) 8012, https://doi.org/10.1038/s41467-024-52254-0.
[23] N. Boers, R.V. Donner, B. Bookhagen, J. Kurths, Complex network analysis helps to identify impacts of the El Niño Southern Oscillation on moisture divergence in South America, Clim. Dyn. 45 (2015) 619–632, https://doi.org/10.1007/s00382-014-2265-7.
[24] Z. Lu, W. Dong, B. Lu, N. Yuan, Z. Ma, M.I. Bogachev, J. Kurths, Early warning of the Indian Ocean Dipole using climate network analysis, Proc Natl Acad Sci. USA 119 (2022), https://doi.org/10.1073/pnas.2109089119.
[25] G. Konapala, S. Mondal, A. Mishra, Quantifying spatial drought propagation potential in North America using complex network theory, Water Resour. Res. 58 (2022), https://doi.org/10.1029/2021WR030914.
[26] N. Boers, B. Goswami, A. Rheinwalt, B. Bookhagen, B. Hoskins, J. Kurths, Complex networks reveal global pattern of extreme-rainfall teleconnections, Nature 566 (2019) 373–377, https://doi.org/10.1038/s41586-018-0872-x.
[27] K. Li, Y. Huang, K. Liu, M. Wang, F. Cai, J. Zhang, N. Boers, Key propagation pathways of extreme precipitation events revealed by climate networks, npj Clim. Atmos. Sci. 7 (2024) 165, https://doi.org/10.1038/s41612-024-00701-6.
[28] S. De, S. Gupta, V.R. Unni, R. Ravindran, P. Kasthuri, N. Marwan, J. Kurths, R.I. Sujith, Study of interaction and complete merging of binary cyclones using complex networks, Chaos 33 (2023) 013129, https://doi.org/10.1063/5.0101714.
[29] S. Gupta, N. Boers, F. Pappenberger, J. Kurths, Complex network approach for detecting tropical cyclones, Clim. Dyn. 57 (2021) 3355–3364, https://doi.org/10.1007/s00382-021-05871-0.
[30] M. Ying, W. Zhang, H. Yu, X. Lu, J. Feng, Y. Fan, Y. Zhu, D. Chen, An overview of the China meteorological administration tropical cyclone database, J. Atmos. Ocean. Technol. 31 (2014) 287–301, https://doi.org/10.1175/JTECH-D-12-00119.1.
[31] Xiaoqin Lu, H. Yu, M. Ying, B. Zhao, S. Zhang, L. Lin, L. Bai, R. Wan, Western North Pacific tropical cyclone database created by the China meteorological administration, Adv. Atmos. Sci. 38 (2021) 690–699, https://doi.org/10.1007/s00376-020-0211-7.
[32] J. Studholme, A.V. Fedorov, S.K. Gulev, K. Emanuel, K. Hodges, Poleward expansion of tropical cyclone latitudes in warming climates, Nat. Geosci. 15 (2022) 14–28, https://doi.org/10.1038/s41561-021-00859-1.
[33] E.K.M. Chang, Y. Guo, Is the number of North Atlantic tropical cyclones significantly underestimated prior to the availability of satellite observations? Geophys. Res. Lett. 34 (2007) https://doi.org/10.1029/2007GL030169.
[34] G.D. Atkinson, C.R. Holliday, Tropical Cyclone Minimum Sea Level pressure-maximum Sustained Wind Relationship for Western North Pacific, 1975.
[35] M.K. Tippett, S.J. Camargo, A.H. Sobel, A poisson regression index for tropical cyclone genesis and the role of large-scale vorticity in genesis, J. Clim. 24 (2011) 2335–2357, https://doi.org/10.1175/2010JCLI3811.1.
[36] H. Hersbach, B. Bell, P. Berrisford, G. Biavati, A. Horányi, J. Muñoz Sabater, J. Nicolas, C. Peubey, R. Radu, I. Rozum, D. Schepers, A. Simmons, C. Soci, D. Dee, J.-N. Thépaut, ERA5 hourly data on single levels from 1940 to present. https://doi.org/10.24381/cds.adbb2d47, 2023.
[37] H. Hersbach, B. Bell, P. Berrisford, G. Biavati, A. Horányi, J. Muñoz Sabater, J. Nicolas, C. Peubey, R. Radu, I. Rozum, D. Schepers, A. Simmons, C. Soci, D. Dee, J.-N. Thépaut, ERA5 hourly data on pressure levels from 1940 to present. https://doi.org/10.24381/cds.bd0915c6, 2023.
[38] R. Quian Quiroga, T. Kreuz, P. Grassberger, Event synchronization: a simple and fast method to measure synchronicity and time delay patterns, Phys. Rev. E 66 (2002) 041904, https://doi.org/10.1103/PhysRevE.66.041904.
[39] P. Qiao, Z. Gong, W. Liu, Y. Zhang, G. Feng, W. Dong, Extreme rainfall synchronization network between Southwest China and Asia–Pacific region, Clim. Dyn. 57 (2021) 3207–3221, https://doi.org/10.1007/s00382-021-05865-y.
[40] P. Jaccard, The distribution OF the FLORA IN the ALPINE ZONE, [1], New Phytologist 11 (1912) 37–50, https://doi.org/10.1111/j.1469-8137.1912.tb05611.x.
[41] K. Hodges, A. Cobb, P.L. Vidale, How well are tropical cyclones represented in reanalysis datasets? J. Climate 30 (2017) 5243–5264, https://doi.org/10.1175/JCLI-D-16-0557.1.
[42] K. Bi, L. Xie, H. Zhang, X. Chen, X. Gu, Q. Tian, Accurate medium-range global weather forecasting with 3D neural networks, Nature 619 (2023) 533–538, https://doi.org/10.1038/s41586-023-06185-3.
[43] R. Lam, A. Sanchez-Gonzalez, M. Willson, P. Wirnsberger, M. Fortunato, F. Alet, S. Ravuri, T. Ewalds, Z. Eaton-Rosen, W. Hu, A. Merose, S. Hoyer, G. Holland, O. Vinyals, J. Stott, A. Pritzel, S. Mohamed, P. Battaglia, Learning skillful medium-range global weather forecasting, Science 382 (2023) 1416–1421, https://doi.org/10.1126/science.adi2336.
[44] Q. Wang, D. Zhao, Y. Duan, H. Wang, Z. Sun, Y. Xu, Observational fine-scale evolutionary characteristics of concentric eyewall Typhoon Doksuri (2023), Atmos. Res. 310 (2024) 107630, https://doi.org/10.1016/j.atmosres.2024.107630.
[45] K. Kim, S.-J. Lee, K.-M. Shim, Model prediction and evaluation of wind damage in major crops caused by a typhoon (Khanun), Korean Journal of Agricultural and Forest Meteorology 26 (2024) 303–317, https://doi.org/10.5532/KJAFM.2024.26.4.303.
[46] R. Guo, R. Yu, M. Yang, G. Chen, C. Chen, P. Chen, X. Huang, X. Zhang, Analysis of characteristics and evaluation of forecast accuracy for Super Typhoon Doksuri, Trop. Cycl. Res. Rev. 13 (2023) 219–229, https://doi.org/10.1016/j.tcrr.2024.09.001.
[47] S.J. Camargo, A.H. Sobel, Western North Pacific tropical cyclone intensity and ENSO, J. Clim. 18 (2005) 2996–3006, https://doi.org/10.1175/JCLI3457.1.
[48] C. Wang, C. Li, M. Mu, W. Duan, Seasonal modulations of different impacts of two types of ENSO events on tropical cyclone activity in the western North Pacific, Clim. Dyn. 40 (2013) 2887–2902, https://doi.org/10.1007/s00382-012-1434-9.